The study of heat flux for disruption on experimental advanced superconducting tokamak

Zhendong Yang' , Jianan Fang' , Xianzu Gong, Kaifu Gan, Jiarong Luo, Hailin Zhao, Zhixue Cui, Bin Zhang, and Meiwen Chen

Citation: Physics of Plasmas **23**, 052502 (2016); doi: 10.1063/1.4948494
View online: http://dx.doi.org/10.1063/1.4948494
View Table of Contents: http://aip.scitation.org/toc/php/23/5
Published by the American Institute of Physics

The study of heat flux for disruption on experimental advanced superconducting tokamak

Zhendong Yang,[1,2,a)] Jianan Fang,[1,a)] Xianzu Gong,[2] Kaifu Gan,[2] Jiarong Luo,[1] Hailin Zhao,[2] Zhixue Cui,[1] Bin Zhang,[2] and Meiwen Chen[2]
[1]*College of Information Sciences and Technology, Donghua University, Shanghai 201620, China*
[2]*Institute of Plasma Physics, Chinese Academy of Sciences, Hefei 230031, China*

(Received 15 December 2015; accepted 19 April 2016; published online 3 May 2016)

Disruption of the plasma is one of the most dangerous instabilities in tokamak. During the disruption, most of the plasma thermal energy is lost, which causes damages to the plasma facing components. Infrared (IR) camera is an effective tool to detect the temperature distribution on the first wall, and the energy deposited on the first wall can be calculated from the surface temperature profile measured by the IR camera. This paper concentrates on the characteristics of heat flux distribution onto the first wall under different disruptions, including the minor disruption and the vertical displacement events (VDE) disruption. Several minor disruptions have been observed before the major disruption under the high plasma density in experimental advanced superconducting tokamak. During the minor disruption, the heat fluxes are mainly deposited on the upper/lower divertors. The magnetic configuration prior to the minor disruption is a lower single null with the radial distance between the two separatrices in the outer midplane $dR_{sep} = -2$ cm, while it changes to upper single null ($dR_{sep} = 1.4$ cm) during the minor disruption. As for the VDE disruption, the spatial distribution of heat flux exhibits strong toroidal and radial nonuniformity, and the maximum heat flux received on the dome plate can be up to 11 MW/m^2. *Published by AIP Publishing.* [http://dx.doi.org/10.1063/1.4948494]

I. INTRODUCTION

Major disruption is one of the most dangerous events in the tokamak. The damages of disruption are mainly from the thermal quench and current quench. During the thermal quench, most of the thermal energy is quickly lost, due to the small time scale (several ms) of the heat flux onto the plasma facing components (PFCs), which results in the sharp increase of temperature of the first wall and damages to PFCs. In ITER, the energy fluxes onto the PFCs during disruption are about tens of GW/m^2.[1] During the current quench, the $J \times B$ forces from the halo current and eddy current induced on the in-vessel chamber could deform the vessel structure.[2] Furthermore, the generation of runaway electrons during the current quench may cause severe damage to the PFCs.[3] Generally, the potential damage to the first wall from the plasma disruption is increased as the plasma stored energy and plasma current increase. Therefore, understanding the characteristic and dynamics of the plasma disruption in tokamaks is very essential to avoid or ameliorate the damage to the PFCs, especially for the next-step tokamak devices, such as ITER and demonstration fusion reactor (DEMO).

Many causes of the plasma disruption in tokamaks, such as low-q, locked mode, density limit, high beta, and vertical displacement event (VDE),[4] have been reported up to now. It is found that a series of minor disruptions occur before the occurrence of the major disruption in high density discharges. A study on the main characteristics of the minor disruption can give us hints on how to reduce the damage to the PFCs, and how to control and avoid the last major disruption. VDE disruption, which is caused by the loss of the control of the plasma position, is considered to be the most dangerous disruption in tokamaks. Study on the main characteristics of the VDE disruption is very essential to estimate and to reduce the potential damage to the PFCs.

In order to mitigate the disruption damage, a wide variety of methods, such as massive gas injection (MGI),[5] killer pellet injection, and large shattered cryogenic pellet injection (SPI),[6] have been used for rapid shut down of tokamaks. Meanwhile, to understand the characteristic and dynamics of the plasma disruption, some effective diagnostics, including soft x-ray arrays[7] for thermal quench time determination, absolute extreme ultraviolet (AXUV)[8] for radiation power measurements, electron cyclotron emission (ECE) diagnostic,[9] and infrared (IR) camera and visible camera,[10,11] should be used for disruption studies.

During the 2014 experimental advanced superconducting tokamak (EAST) campaign, the IR viewing system installed on EAST allows a view of both the main chamber and divertor plate, which makes it possible to study the characteristic of heat flux during the disruption. In this paper, the main characteristics of heat flux onto the divertor in the minor disruption and that in the VDE disruption are studied. Several minor disruptions have been observed under high density plasma discharge. During the minor disruption, the heat fluxes are mainly deposited on the upper/lower divertors. The magnetic configuration prior to the minor disruption is lower single null with the radial distance between the two separatrices in the outer midplane $dR_{sep} = -2$ cm, while

a)Authors to whom correspondence should be addressed. Electronic addresses: dongyz@ipp.ac.cn and jafang@dhu.edu.cn.

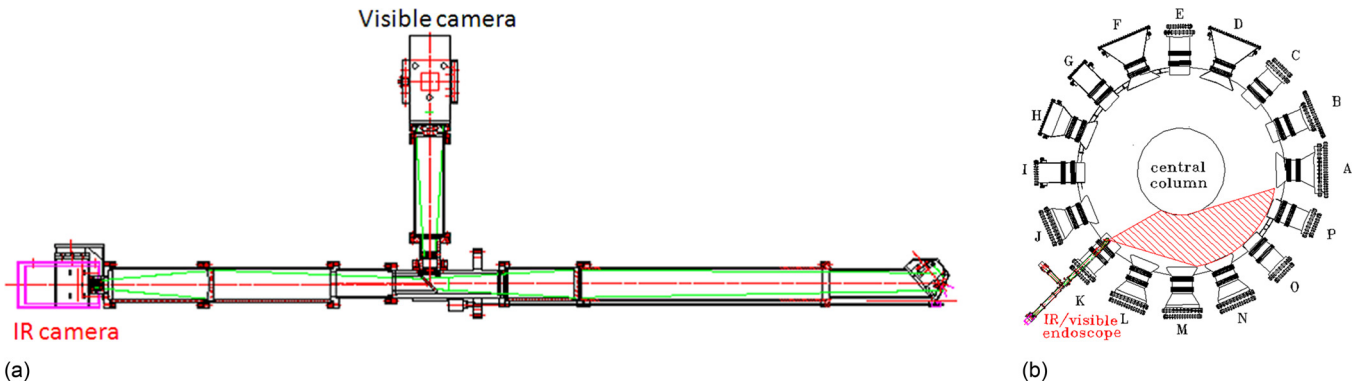

FIG. 1. (a) IR/visible endoscope system. (b) Top view of IR/visible endoscope in EAST.

during the minor disruption it changes to upper single null ($dR_{sep} = 1.4$ cm). For the VDE disruption, the spatial distribution of the heat flux shows strong toroidal and radial non-uniformity. This paper is organized as follows. Section II briefly introduces the main diagnostic systems and the experimental setup. Section III discusses the characteristics of minor disruption, and Section IV discusses the characteristics of heat flux distribution on the divertor under the VDE disruption. Finally, the summary and conclusions are given in Section V.

II. DIAGNOSTICS AND EXPERIMENTAL SETUP

Experimental Advanced Superconducting Tokamak (EAST) is a fully superconducting tokamak, aimed at achieving high power and long pulse steady-state operation.[12] Its basic parameters are the major radius R $\sim$ 1.75 m, minor radius a $\sim$0.45 m, maximum plasma current $\sim$1 MA, and maximum toroidal field $\sim$3.5 T. In the 2014 EAST campaign, many auxiliary heating systems such as low hybrid wave (LHW), ion cyclotron radio frequency (ICRF), and neutral beam injection (NBI) have been applied to improve the plasma performance, and some effective diagnostic systems, such as ECE, AXUV,[13,14] and IR camera, are installed on EAST device, which can be used for the disruption study.

The IR/visible endoscope system consists of the IR camera, the visible camera, and the spectroscope (Fig. 1(a)). This system has been installed on K port of EAST device (Fig. 1(b)) for the first time in 2014 EAST campaign. In this diagnostic system, the IR camera and visible camera have the same field of view as shown in Figs. 1 (IR camera) and 2 (visible camera), respectively. The mid-wave infrared (MWIR) camera is used to measure the IR radiation in the wavelength range of 3–5 μm. The maximum frame rate of the MWIR camera is 2.9 kHz for a 132 $\times$ 3 pixels sub-window and 115 Hz for full-frame (640 $\times$ 512 pixels) data acquisition. The maximum frame rate at full resolution (1280 $\times$ 800 pixels) of the phantom V710 visible camera is up to 7530 kHz. The wide field of view (47° $\times$ 58°) of the diagnostic system makes it possible to monitor the temperature evolution on the upper divertor targets, lower divertor targets, high field side (HFS), and the limiter simultaneously. The spatial resolution of the diagnostic system along the divertor plate in the poloidal direction is 4 mm for the IR camera and 3 mm for the visible camera.

Electron Cyclotron Emission (ECE) radiometer is an effective tool to provide the temporal evolution of the local

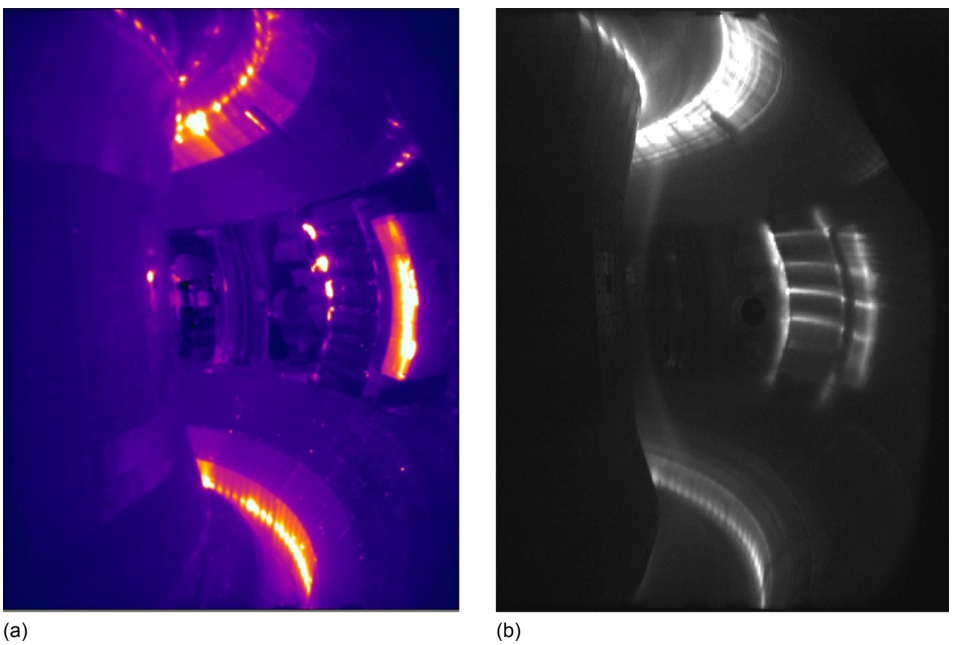

FIG. 2. (a) Field of view with IR camera and (b) field of view with visible camera.

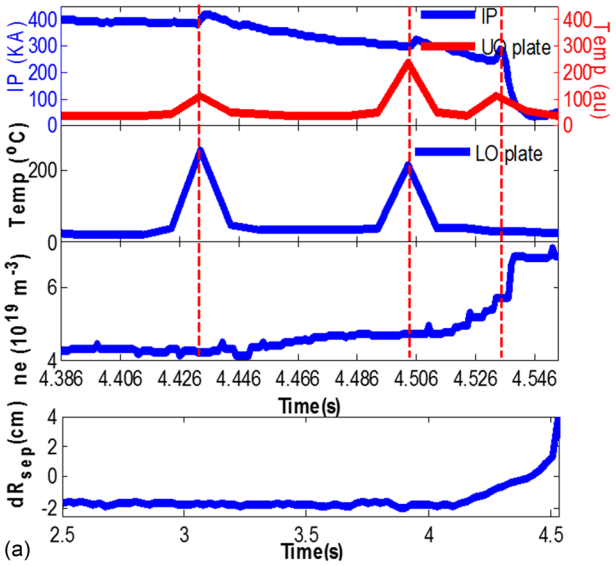

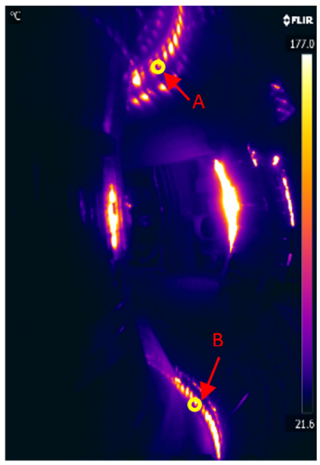

FIG. 3. (a) The blue line shows the time evolution of the plasma current and the red line shows the time evolution of the point A temperature on the upper outer divertor plate; (b) the time evolution of the point B temperature on the lower outer divertor plate; (c) the time evolution of the central line average electron density; and (d) $dR_{sep} = R_{sep\_L}$-R_{sep_U}.

electron temperature and the electron temperature profile. In EAST, the 32-channel heterodyne radiometer has been installed in 2014 experiment campaign. This system collects X-mode ECE radiation spanning from 104 GHz to 168 GHz, covering radial spanning r/a from −1.0 to 1.0 at a toroidal magnetic field of 2.3 T. Its maximum temporal and radial resolutions are about 2.5 μs and 1 cm, respectively. More details of the EAST ECE system can be found in Refs. 15 and 16.

III. CHARACTERISTICS OF MINOR DISRUPTION

In the high plasma density discharges, a series of minor disruptions are often found to occur before the occurrence of the last major disruption. Study on the main characteristics of the minor disruption can give us hints on how to reduce the damage to the PFCs and how to control or avoid the last major disruption. To illustrate the main characteristics of the minor disruptions of EAST discharges with high plasma density, we take shot 48661 as an example. The main parameters of this discharge are as follows: the plasma current Ip ∼ 400 kA, the toroidal magnetic field Bt = 2.3 T, and the line-averaged density ne ≈ 4.2×10^{19} m^{-3}. The magnetic configuration is a lower single null prior to the minor disruption where the dR_{sep} is about −2 cm. During the minor disruption, the magnetic configuration changes to a double null at 4.43 s (dR_{sep} = 0 cm) and upper single null at 4.50 s(dR_{sep} = 1.4 cm). In this shot, two minor disruptions occur at t = 4.43 s and t = 4.50 s, respectively, and the last major disruption occurs at t = 4.53 s, just as Figs. 3 and 4 show. The characteristics of the minor disruptions mainly indicate in two aspects, i.e., plasma current falls slightly and the temperature of divertor plate increases rapidly. During each minor disruption, the plasma current falls by ∼20% as is illustrated in Fig. 3(a). Meanwhile, the heat fluxes mainly deposit on the upper/lower divertor plate (Fig. 4), which is indicated by the increase tendency of the temperature of the divertor plate (Figs. 3(a) and 3(b)). For the last major disruption at t = 4.53 s, the temperature on the upper divertor plate increases only slightly due to the energy lost during the two minor disruptions, as is represented by the red line in Fig. 3(a).

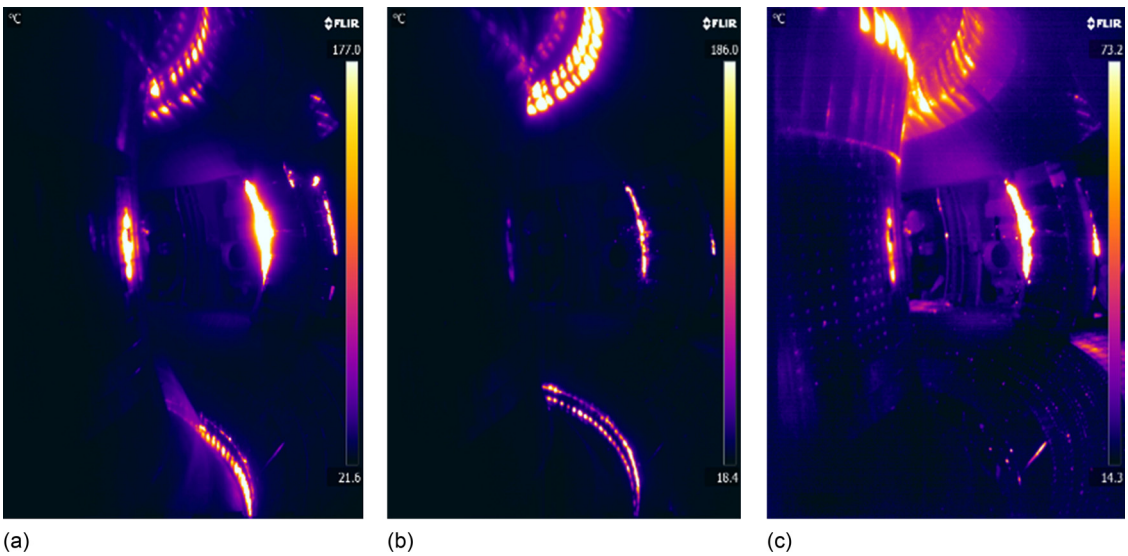

FIG. 4. IR image for the shot 48 661: (a) at t = 4.43 s, (b) t = 4.50 s, and (c) t = 4.53 s.

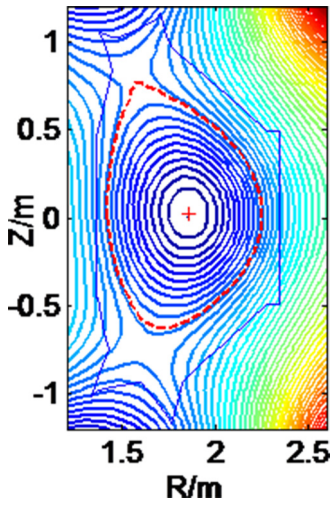

FIG. 5. The plasma equilibrium reconstruction of shot 46 881 at 4500 ms.

Here, in the following part, some interpretations to the characteristics of the minor disruptions described above will be given. Due to a sudden large heat flux from the core plasma towards the plasma edge and also due to that the magnetic field has not been severely disrupted, the heat fluxes mainly deposit onto the upper/lower divertor plate during the minor disruption. The fact that the magnetic field has not been severely disrupted can be demonstrated by the equilibrium reconstruction of magnetic field in Fig. 5 and large heat flux from the core plasma towards the plasma edge can be demonstrated by the ECE diagnostic as shown in Fig. 6. In Fig. 6, the temporal evolution of the local electron temperature in a radial position R from 1.4642 m to 2.0837 m is shown for the shot 48661. The electron temperature of the core region (R = 1.6992–1.9776 m) is decreased at 4.42 s, 4.492 s, and 4.52 s, marked by A, B, and C, respectively, while the electron temperature in lower field side (R = 2.0177 m–2.0837 m) and the high field side (R = 1.4642 m–1.6510 m) is increased, which indicates that the heat flux is directed to the plasma edge during the minor disruption and is consistent with the increase tendency of the divertor temperature detected by the IR camera. That is to say, during the minor disruption, the sudden large heat fluxes from the core plasma directly flow towards the plasma edge, causing the temperature of the divertor to increase rapidly, and also, not so severe disruption of the magnetic field, so that the heat flux mainly deposits onto the upper/lower divertors plate.

The sudden increase of the temperature on the divertor during the minor disruption before the major disruption is a useful signal to foresee the collapse of the plasma and to take measure to alleviate the damage to PFCs. What is more, the strong interaction between plasmas and the first wall during the minor disruption has been observed and is shown in Fig. 7. During the minor disruption, the visible radiation intensity from the divertor increases suddenly which is illustrated by the red line in Fig. 7(a). As the maximum frame rate can reach up to be more than 100 kHz, the visible camera is able to acquire the signal quickly enough to foresee the collapse of the plasma.

IV. VDE DISRUPTION

In a VDE, the position control is lost and the plasma moves vertically either up or down. When the plasma collides with the top or bottom of the vessel, the temperature of the first wall will have a large increase, which is a serious

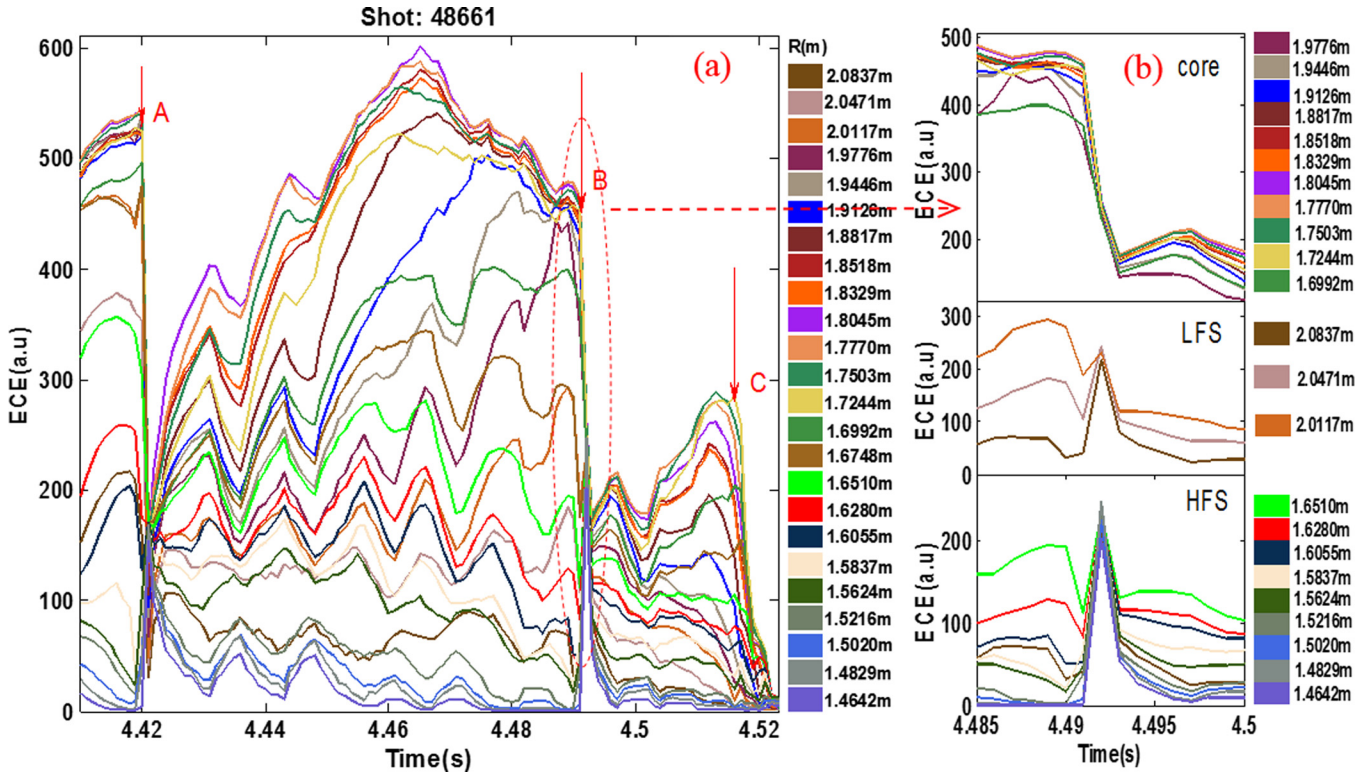

FIG. 6. (a) ECETe(r,t) is shown by color online. (b) Te(r,t) from 4.485 s to 4.500 s. The channels position is indicated at the right.

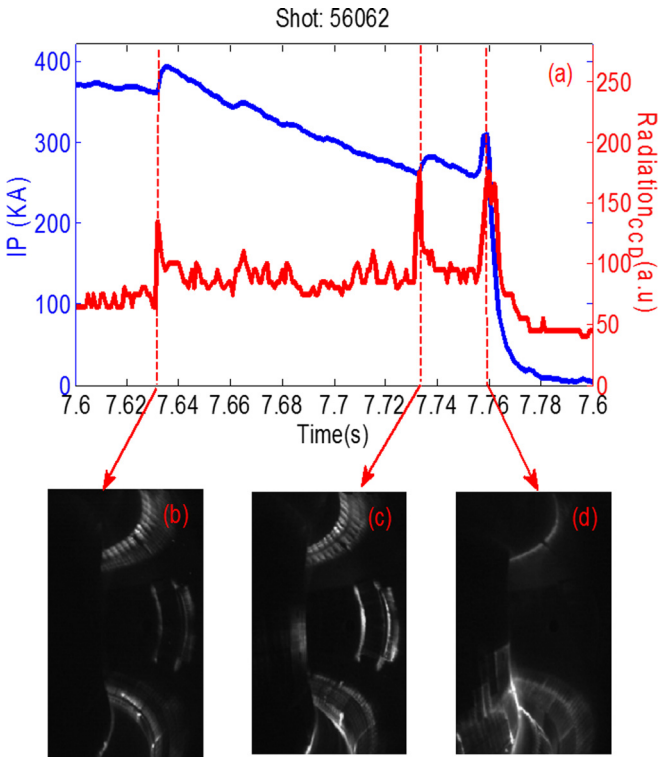

FIG. 7. (a) The blue line shows the evolution of the plasma current and the red line shows the evolution of the visible radiation on the lower outer divertor; (b) the visible image at 7.632 s; (c) the visible image at 7.733 s; and (d) the visible image at 7.760 s.

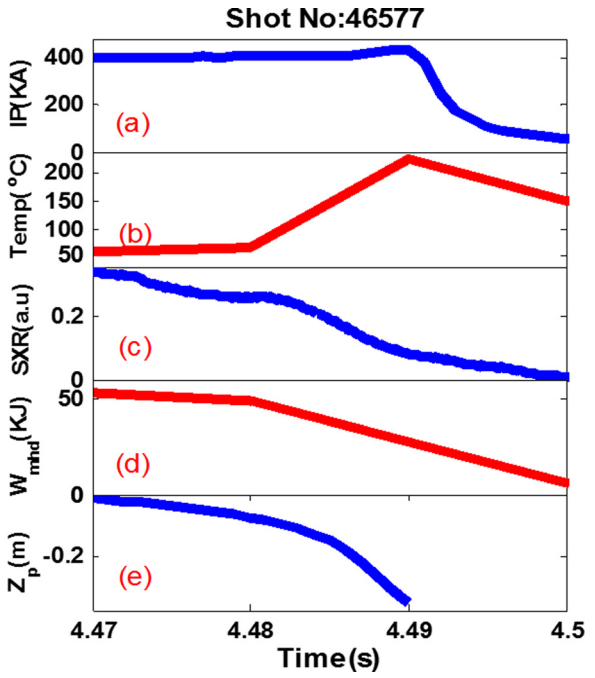

FIG. 9. (a) Plasma current; (b) the time evolution of temperature on the lower dome; (c) Soft x-ray (SXR) emission on a central; (d) the plasma thermal energy; and (e) the vertical position of the plasma center.

problem to the PFCs. Study on the main characteristics of the VDE disruption is very essential to estimate and to reduce the potential damage to the PFCs. To illustrate the main characteristics of the VDE disruptions on EAST, we take shot 46577 as an example. The discharge parameters are $Ip = 400\,kA$, $ne = 2.9 \times 10^{19}\,m^{-3}$, $BT = 2.3\,T$, and lower hybrid wave heating power up to 0.6 MW.

From the visible and IR image (Fig. 8), it can be seen that there is a large increase on the temperature of the lower divertor during the VDE disruption. The peak temperature of the lower dome plate increases from 70 °C to 230 °C within a short time scale (10 ms), as shown in Fig. 9. In order to study the characteristics of the VDE disruption, the power density on the divertor need to be deduced. In the EAST, the carbon is used on the lower divertor. The thermal diffusivity of the material is given by $\alpha = k/(\rho \times c_p)$, where k, ρ, and c_p are the thermal conductivity, density, and heat capacity, respectively. For the carbon on the lower divertor, α is $1.3 \times 10^{-4}\,m^2/s$. Since the temperature of the first wall increases rapidly, the time scale is very short. The heat diffusivity of carbon is so lower that the temperature would diffuse on several hundred micrometers in 10 ms, which is lower than the spatial resolution of the IR camera at the dump (4 mm). So, the

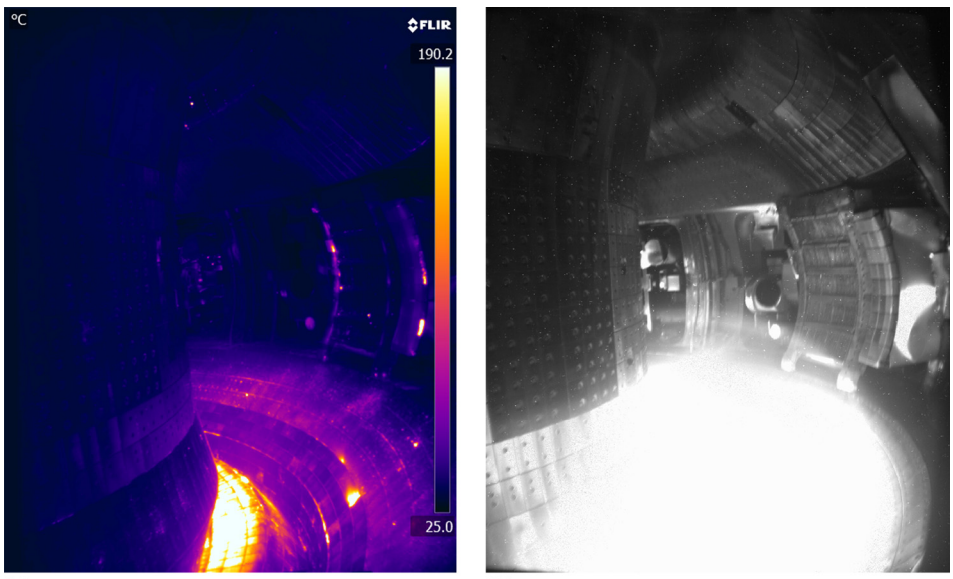

FIG. 8. Visible (right) and IR image during the VDE disruption.

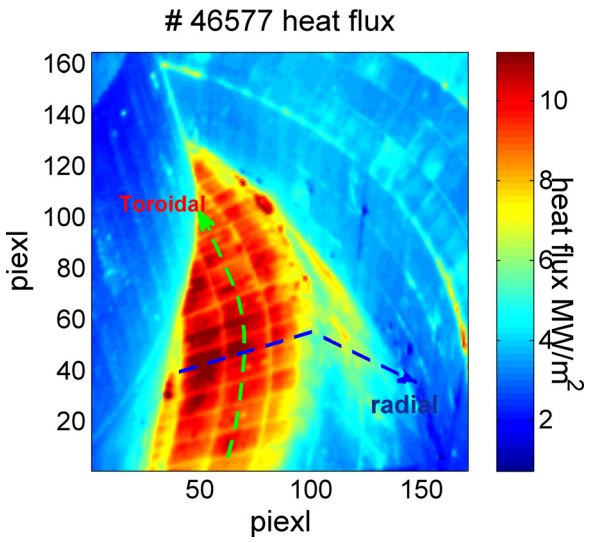

FIG. 10. The heat flux on the lower dome during the VDE.

lateral diffusion can be neglected and the heat flux on the divertor can be calculated by solving the one-dimensional analytical formula. The heat flux on the lower dome during the VDE disruption is given in Fig. 10, and the peak heat flux onto the dome plate is about 11 MW/m^2. Fig. 11 illustrates the inhomogeneous distributions of the heat flux on the dome plate along specific radial and toroidal directions (corresponding to the blue and green curves in Fig. 10), in which the ratio between the maximum and minimum value of the heat flux is 2 in the radial direction and 1.2 in the toroidal direction. Also, the peak density of heat flux onto the dome plate is about 11 MW/m^2, which is not very high due to the low total heating power of 1 MW only. However, to achieve discharges with high plasma performances in EAST, the heating power will be increased up to 20 MW. Since the

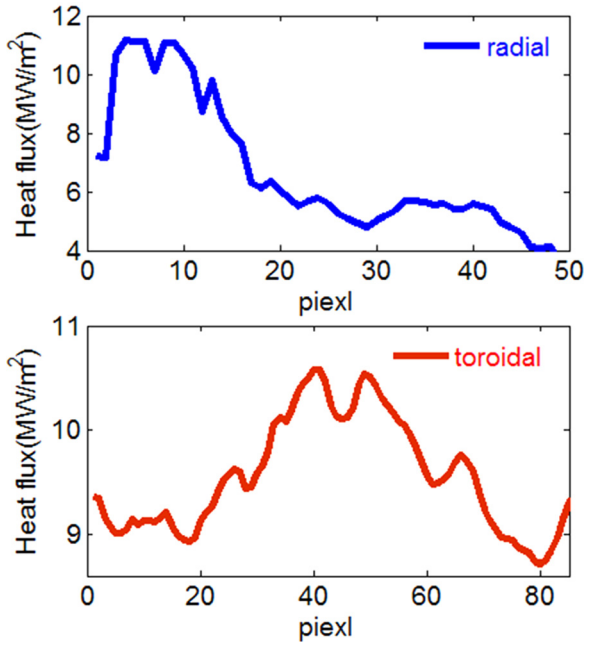

FIG. 11. The heat flux on lower dome plate along the disruption radial and toroidal directions.

potential damage to the first wall from the plasma disruption increases as the plasma stored energy and plasma current increase, studying the plasma disruption is very essential to acquire long-pulse/steady-state operation of EAST. Also, to understand the physics mechanism of plasma disruption and to realize the control of plasma disruption in EAST, further research work is still needed.

V. CONCLUSIONS

The IR/visible endoscope system is first used on EAST in 2014 which allows the direct observation of the power conduction on the PFCs. Some minor disruptions have been observed under the high density plasma discharge. During the minor disruption, the heat fluxes are mainly deposited onto the upper/lower divertor plate. This is mainly due to a sudden large heat flux from the core plasma towards the plasma edge, and the magnetic field of plasma edge has not been disrupted during the minor disruption. This phenomenon is also detected by the visible camera. As the maximum frame rate of the high-speed visible camera reaches up to 100 kHz and beyond, the visible radiation intensity increased suddenly on the divertor during the minor disruption is a useful signal to foresee the collapse of the plasma. In a VDE disruption, the spatial distribution of heat flux exhibits strong toroidal and radial nonuniformity, and the maximum heat flux received on the dome plate can be up to 11 MW/m^2.

ACKNOWLEDGMENTS

This work was supported by the National Magnetic Confinement Fusion Science Program of China (Contract Nos. 2014GB101002, 2013GB102001, and 2015GB102001).

[1]ITER Physics Expert Group on Divertor, ITER Physics Expert Group on Divertor Modelling and Database, and ITER Physics Basis Editors, Nucl. Fusion **39**, 2391 (1999).
[2]V. Riccardo, T. C. Hender, P. J. Lomas, B. Alper, T. Bolzonella, P. de Vries, G. P. Maddison, and JET EFDA Contributors, Plasma Phys. Controlled Fusion **46**, 925–934 (2004).
[3]R. Nygren, T. Lutz, D. Walsh, G. Martin, M. Chatelier, T. Loarer, and D. Guilhem, J. Nucl. Mater. **241–243**, 522–527 (1997).
[4]T. C. Hender, J. C. Wesley, J. Bialek, A. Bondeson, A. H. Boozer, R. J. Buttery, A. Garofalo, T. P. Goodman, R. S. Granetz, Y. Gribov, O. Gruber, M. Gryaznevich, G. Giruzzi, S. Günter, N. Hayashi, P. Helander, C. C. Hegna, D. F. Howell, D. A. Humphreys, G. T. A. Huysmans, A. W. Hyatt, A. Isayama, S. C. Jardin, Y. Kawano, A. Kellman, C. Kessel, H. R. Koslowski, R. J. La Haye, E. Lazzaro, Y. Q. Liu, V. Lukash, J. Manickam, S. Medvedev, V. Mertens, S. V. Mirnov, Y. Nakamura, G. Navratil, M. Okabayashi, T. Ozeki, R. Paccagnella, G. Pautasso, F. Porcelli, V. D. Pustovitov, V. Riccardo, M. Sato, O. Sauter, M. J. Schaffer, M. Shimada, P. Sonato, E. J. Strait, M. Sugihara, M. Takechi, A. D. Turnbull, E. Westerhof, D. G. Whyte, R. Yoshino, H. Zohm, and ITPA MHD, Disruption and Magnetic Control Topical Group, Nucl. Fusion **47**, S128 (2007).
[5]P. L. Taylor, A. G. Kellman, T. E. Evans, D. S. Gray, D. A. Humphreys, A. W. Hyatt, T. C. Jernigan, R. L. Lee, J. A. Leuer, S. C. Luckhardt, P. B. Parks, M. J. Schaffer, D. G. Whyte, and J. Zhang, Phys. Plasmas **6**, 1872 (1999).
[6]L. R. Baylor, S. K. Combs, C. R. Foust, T. C. Jernigan, S. J. Meitner, P. B. Parks, J. B. Caughman, D. T. Fehling, S. Maruyama, A. L. Qualls, D. A. Rasmussen, and C. E. Thomas, Nucl. Fusion **49**, 085013 (2009).
[7]M. Lehnen, A. Alonso, G. Arnoux, N. Baumgarten, S. A. Bozhenkov, S. Brezinsek, M. Brix, T. Eich, S. N. Gerasimov, A. Huber, S. Jachmich, U. Kruezi, P. D. Morgan, V. V. Plyusnin, C. Reux, V. Riccardo, G. Sergienko, M. F. Stamp, and JET EFDA Contributors, Nucl. Fusion **51**, 123010 (2011).

[8]M. L. Reinke, D. G. Whyte, R. Granetz, and I. H. Hutchinson, Nucl. Fusion **48**, 125004 (2008).
[9]A. Krämer-Flecken, K. H. Finken, V. S. Udintsev, H. Larue, and TEXTOR Team, Nucl. Fusion **43**, 1437–1445 (2003).
[10]P. Andrew, A. Alonzo, G. Arnoux, E. Gauthier, J. I. Paley, V. Riccardo, and JET EFDA Contributors, J. Nucl. Mater. **363–365**, 1006–1010 (2007).
[11]E. Delchambre, G. Counsell, A. Kirk, and F. Lott, J. Nucl. Mater. **363–365**, 1409–1413 (2007).
[12]Baonian Wanfor the EAST and HT-7 Teams and International Collaborators, Nucl. Fusion **49**, 104011 (2009).
[13]H. U. Liqun on behalf of EAST Diagnostic Team and Collaborators, Plasma Sci. Technol. **13**, 125 (2009).
[14]H. Chundong, X. Yahong, X. Yuanlai, L. Sheng, X. Yongjian, L. Lizhen, J. Caichao, S. Peng, G. Yuming, L. Jun, and L. Zhimin, Plasma Sci. Technol. **17**, 817 (2015).
[15]X. Han, X. Liu, Y. Liu, C. W. Domier, N. C. Luhmann, Jr., E. Z. Li, L. Q. Hu, and X. Gao, Rev. Sci. Instrum. **85**, 073506 (2014).
[16]X. Liu, H. L. Zhao, Y. Liu, E. Z. Li, X. Han, C. W. Domier, N. C. Luhmann, Jr., A. Ti, L. Q. Hu, and X. D. Zhang, Rev. Sci. Instrum. **85**, 093508 (2014).